

See discussions, stats, and author profiles for this publication at: <https://www.researchgate.net/publication/277893405>

Conjugated Polymer–Small Molecule Alloy Leads to High Efficient Ternary Organic Solar Cells

ARTICLE *in* JOURNAL OF THE AMERICAN CHEMICAL SOCIETY · JUNE 2015

Impact Factor: 12.11 · DOI: 10.1021/jacs.5b03449 · Source: PubMed

CITATIONS

6

READS

162

7 AUTHORS, INCLUDING:



Jianqi Zhang

National Center for Nanoscience and Techn...

31 PUBLICATIONS 93 CITATIONS

[SEE PROFILE](#)



Kun Lu

University of California, San Diego

37 PUBLICATIONS 366 CITATIONS

[SEE PROFILE](#)



Zaiyu Wang

Xi'an Jiaotong University

6 PUBLICATIONS 6 CITATIONS

[SEE PROFILE](#)



Wei ma

Ecole Normale Supérieure de Paris

5 PUBLICATIONS 6 CITATIONS

[SEE PROFILE](#)

Conjugated Polymer–Small Molecule Alloy Leads to High Efficient Ternary Organic Solar Cells

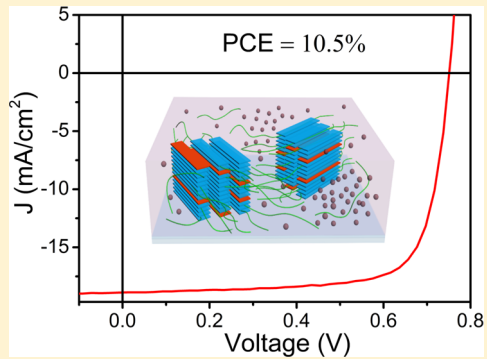
Jianqi Zhang,[†] Yajie Zhang,[†] Jin Fang,[†] Kun Lu,[†] Zaiyu Wang,[‡] Wei Ma,^{*,‡} and Zhixiang Wei^{*,†}

[†]Key Laboratory of Nanosystem and Hierarchical Fabrication, National Center for Nanoscience and Technology, Beijing 100190, P. R. China

[‡]State Key Laboratory for Mechanical Behavior of Materials, Xi'an Jiaotong University, Xi'an 710049, P. R. China

Supporting Information

ABSTRACT: Ternary organic solar cells are promising candidates for bulk heterojunction solar cells; however, improving the power conversion efficiency (PCE) is quite challenging because the ternary system is complicated on phase separation behavior. In this study, a ternary organic solar cell (OSC) with two donors, including one polymer (PTB7-Th), one small molecule (*p*-DTS-(FBTT_H)₂), and one acceptor (PC₇₁BM), is fabricated. We propose the two donors in the ternary blend forms an alloy. A notable averaged PCE of 10.5% for ternary OSC is obtained due to the improvement of the fill factor (FF) and the short-circuit current density (J_{sc}), and the open-circuit voltage (V_{oc}) does not pin to the smaller V_{oc} of the corresponding binary blends. A highly ordered face-on orientation of polymer molecules is obtained due to the formation of an alloy structure, which facilitates the enhancement of charge separation and transport and the reduction of charge recombination. This work indicates that a high crystallinity and the face-on orientation of polymers could be obtained by forming alloy with two miscible donors, thus paving a way to largely enhance the PCE of OSCs by using the ternary blend strategy.



INTRODUCTION

Organic solar cells (OSCs) have made substantial progress recently and have shown their potential in low-cost, flexible, and lightweight solar energy conversion devices.¹ Although OSCs have such advantages, a further increase of their power conversion efficiency (PCE) and stability is needed for future applications. Extensive research efforts aimed at increasing the PCE of OSCs have been devoted to the design and synthesis of new materials,² morphology control and characterization,³ and development of new device architectures.⁴ Thus, high efficiencies have been obtained in the laboratory for single-junction devices (~10%)⁵ and tandem devices (~11%).⁶ To further increase the PCE of single-junction devices, ternary blend systems that contain two donor materials and one fullerene acceptor have been used.⁷ The ternary strategy can increase the fill factor and short-circuit current (J_{sc}) simultaneously by carefully selecting molecules.⁸ Koppe et al. have pointed out that photogenerated positive polarons rapidly transfer from low band gap polymer phase to wide band gap phase,⁹ which explains the increase of short circuit current (J_{sc}) of ternary OSCs. However, the current highest efficiency of ternary solar cells is reported at 8.4%, which is still lower than the highest record of single-junction devices.^{8b} Moreover, most ternary solar cells are based on a conventional device structure instead of an inverted structure, the latter is more stable than the former for real applications.¹⁰ Studies on the new ternary system with inverted structure, as well as their working

mechanism, are of great importance to further increase the efficiency and the stability of OSCs.

The PCE of OSCs is significantly associated with a bicontinuous morphology, which is often classified according to domain size, purity, and crystallinity.¹¹ The crystallinity of the conjugated molecules serves an important function for the above-mentioned morphological characteristics. Conjugated polymers normally have a good compatibility with fullerene acceptors. However, the crystallinity of conjugated polymers is usually low and insufficient to obtain optimal morphology. Meanwhile, small molecules show better crystallinity than polymers and easily causes crystalline domains that are too large, which are not beneficial to charge separation.¹² Therefore, a ternary strategy that adds small molecules into polymers has a great potential to improve the crystallinity of the polymer phase in OSCs. Moreover, the crystallite orientation with respect to the electrodes have been shown to be important in OSCs¹³ and in many other organic electronic devices.¹⁴ Face-on orientation is preferred for single-junction solar cells because this orientation can reduce the recombination of photoexcitons during charge separation.¹⁵ On the other hand, it has been pointed out that the alloy model ternary solar cells have the potential for higher solar cell efficiency than binary blends.¹⁶ Therefore, ternary solar cells fabricated by using two miscible donors, one is a high-performance polymer and

Received: April 2, 2015

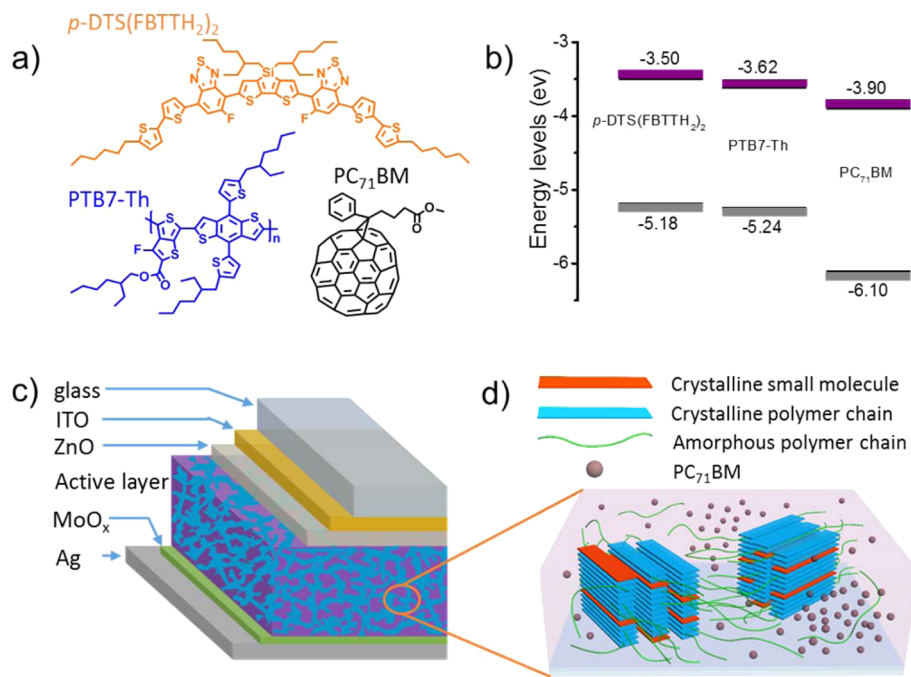


Figure 1. (a) Chemical structures of *p*-DTS(FBTTH₂)₂, PTB7-Th, and PC₇₁BM. (b) Energy level diagrams for *p*-DTS(FBTTH₂)₂, PTB7-Th, and PC₇₁BM. (c) Device structure of the OSC (glass/ITO/ZnO/active layer/MoO_x/Ag). (d) Illustration of the active layer of ternary solar cells, in which the small molecules induce the face-on π - π stacking.

Table 1. Summary of Photovoltaic Parameters of Solar Cells with Different Weight Ratios of *p*-DTS(FBTTH₂) under AM1.5 Illumination at 100 mW/cm²

PTB7-Th:P-DTS(FBTTH ₂):PC ₇₁ BM	V _{oc} (ave) (V)	J _{sc} (ave) (mA/cm ²)	FF (ave) (%)	PCE (ave) (%)
100:0:110	0.805 ± 0.002	17.53 ± 0.21	65.26 ± 0.91	9.20 ± 0.69
95:5:110	0.775 ± 0.003	18.24 ± 0.19	68.81 ± 0.84	9.70 ± 0.14
90:10:110	0.762 ± 0.005	18.26 ± 0.07	74.34 ± 0.64	10.3 ± 0.11
85:15:110	0.755 ± 0.004	18.44 ± 0.04	75.27 ± 0.88	10.5 ± 0.09
80:20:110	0.750 ± 0.013	17.49 ± 0.79	73.61 ± 1.06	9.66 ± 0.56
70:30:110	0.766 ± 0.008	16.67 ± 0.39	70.87 ± 2.29	9.05 ± 0.45
0:100:110	0.711 ± 0.002	12.63 ± 0.30	59.74 ± 2.58	5.40 ± 0.28

another is a high-crystalline small molecule, may form alloy and increased crystallinity simultaneously, which will potentially yield high efficiency ternary OSC.

In this study, a ternary inverted OSC is designed and fabricated by incorporating high crystallinity small molecules into a host binary blend of polymer: [6,6]-phenyl C71 butyric acid methyl ester (PC₇₁BM) system. Poly[4,8-bis(5-(2-ethylhexyl)thiophen-2-yl)benzo[1,2-b:4,5-b']dithiophene-*co*-3-fluorothieno[3,4-*b*]thiophene-2-carboxylate] (PTB7-Th) is selected as the polymer because of a high device efficiency.^{5a,17} 7,7-(4,4-bis(2-Ethylhexyl)-4H-silolo[3,2-b:4,5-b']dithiophene-2,6-diyl)bis(6-fluoro-4-(S'-hexyl-[2,2'-bithiophen]-5-yl)benzo[c] [1,2,5]thiadiazole) (*p*-DTS(FBTTH₂)₂) is selected as the small molecule because of a high crystallinity.¹⁸ The two donors are miscible. The chemical structures of PTB7-Th, *p*-DTS(FBTTH₂)₂, and PC₇₁BM, as well as the corresponding energy levels, are given in Figure 1a and b. We demonstrate that both the crystallinity and the face-on preferential orientation with respect to the substrate are enhanced when the small molecule is added, thus resulting in an average PCE of 10.5% in optimized conditions. The binary system based on PTB7-Th:PC₇₁BM exhibits an average PCE of 9.2%, whereas the ternary system increased to 10.5% by adding a 15% weight ratio of *p*-DTS(FBTTH₂)₂. The hole mobilities and FFs of the

ternary devices are improved compared with that of binary ones, thus resulting higher PCEs.

RESULTS AND DISCUSSION

Device Performance of OSCs. Binary and ternary OSCs were fabricated with inverted architectures of indium tin oxide/ZnO/active layer/MoO_x/Ag (Figure 1c). Figure 1b shows the energy levels of the active layer materials that were determined by using the electrochemical method (Supporting Information Figure S1). The ZnO electron extraction layer was deposited by using sol-gel techniques.¹⁹ After active layer spin coating, the MoO_x hole extraction layer was vacuum deposited, followed by the Ag anode. The influences of the *p*-DTS(FBTTH₂)₂ to PTB7-Th ratios were examined carefully. The overall donors to PC₇₁BM ratio were kept at 1:1.1 in this study. To obtain an optimum bicontinuous morphology, diiodooctane (DIO) was used as an additive. The PCE of the binary and ternary OSCs at different contents of small molecules are summarized in Table 1. The results with a mask are given in Table S1 (Supporting Information). All the masked and unmasked tests had consistent results with relative errors within 5%. The PCE of the ternary system is significantly enhanced compared with binary system. The higher ratios (e.g., larger than 20%) of *p*-DTS(FBTTH₂)₂ induce a macrophase separation of the active

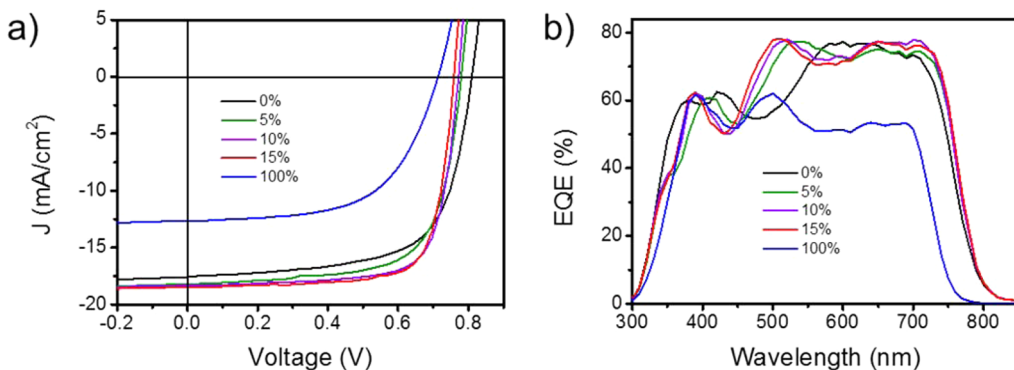


Figure 2. (a) J – V curve of binary and ternary system under AM1.5G illumination from a calibrated solar simulator with an irradiation intensity of 100 mW/cm². The weight ratio of p -DTS(FBTTH₂)₂ for each curve is 0% (black), 5% (green), 10% (violet), 15% (red), and 100% (blue), respectively. (b) EQE curves of the OSCs corresponding to the devices in (a).

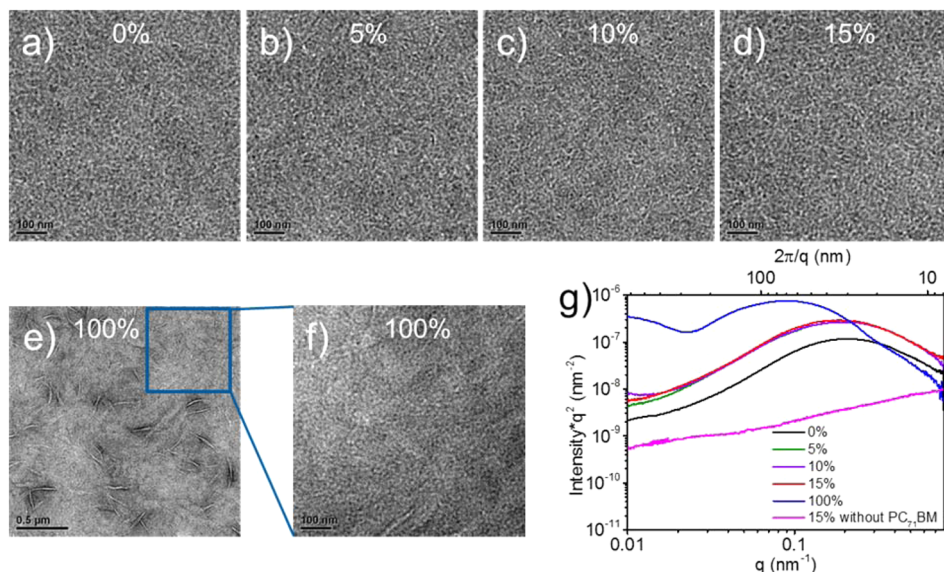


Figure 3. TEM images of OSCs with different contents of p -DTS(FBTTH₂)₂. (a) 0%, (b) 5%, (c) 10%, (d) 15%, (e) 100%, and (f) 100% in a large magnification. The scale bar was indicated in each image. (g) R-SoXS profiles in log scale for binary and ternary systems.

layer (Supporting Information Figure S2). Although the PCE of the ternary system at 20% is higher than that of polymer, the domains formed by the small molecule due to macrophase separation are much higher (around 1 μ m) than the other parts of the thin film. It means that the film thickness is not homogeneous, which hinders the further analysis the results like SCLC, which significantly depends on the film thickness. Herein, the performance of the ternary system at 5%, 10%, and 15% weight ratio of p -DTS(FBTTH₂)₂ is studied carefully.

Figure 2a shows the typical current density versus the voltage (J – V) characteristics of binary and ternary OSCs under AM 1.5 G illuminations at 100 mW/cm². The black and blue curves indicate the photovoltaic performance of polymer (PTB7-Th:PC₇₁BM) and small molecule (p -DTS-(FBTTH₂)₂:PC₇₁BM), respectively. For the polymer system, the devices exhibit an average PCE of 9.2% with $V_{oc} = 0.805$ V, $J_{sc} = 17.53$ mA cm⁻², and FF = 65.26%; for small molecule, the devices show an average PCE of 5.4%, with $V_{oc} = 0.711$ V, $J_{sc} = 12.63$ mA cm⁻², and FF = 59.74%. The red curve presents the J – V characteristic of ternary OSC with a weight ratio of 15%, which has the average PCE of 10.5% for ternary systems with $V_{oc} = 0.755$ V, $J_{sc} = 18.44$ mA cm⁻², and FF = 75.27%. One of our best cells was sent to an accredited solar cell calibration

laboratory (National Center of Supervision and Inspection on Solar Photovoltaic Products Quality, China) for certification, confirming an efficiency of 10.1%, with $V_{oc} = 0.752$ V, $I_{sc} = 0.0007258$ A, FF = 75.71%, area = 0.0409 cm², (Supporting Information Figure S3). Thus, the PCE of the ternary system can be significantly enhanced by incorporating high-crystalline small molecule into the host polymer. The V_{oc} is slightly decreased; however, the J_{sc} and FF are substantially improved by 5.2% and 15.3% (Table 1), respectively, compared with the reference device PTB7-Th:PC₇₁BM. Therefore, the loss of the V_{oc} can be compensated by an increase in J_{sc} and FF, resulting in an increase of PCE by 14.1%. This result indicates a synergistic effect of the small molecule and polymer for the charge separation and transport of the active layer. The external quantum efficiency (EQE) of the ternary blend devices is presented in Figure 2b. The EQE values are enhanced in the region between 450 to 550 nm where PC₇₁BM exhibits a high absorption because p -DTS(FBTTH₂)₂ is incorporated. EQE values show a little red shift which is consistent with the UV-vis absorption spectra (Supporting Information Figure S4).

Morphology and Phase Separation. To study the influence of the morphology by adding p -DTS(FBTTH₂)₂ to PTB7-Th, transmission electron microscopy (TEM) and

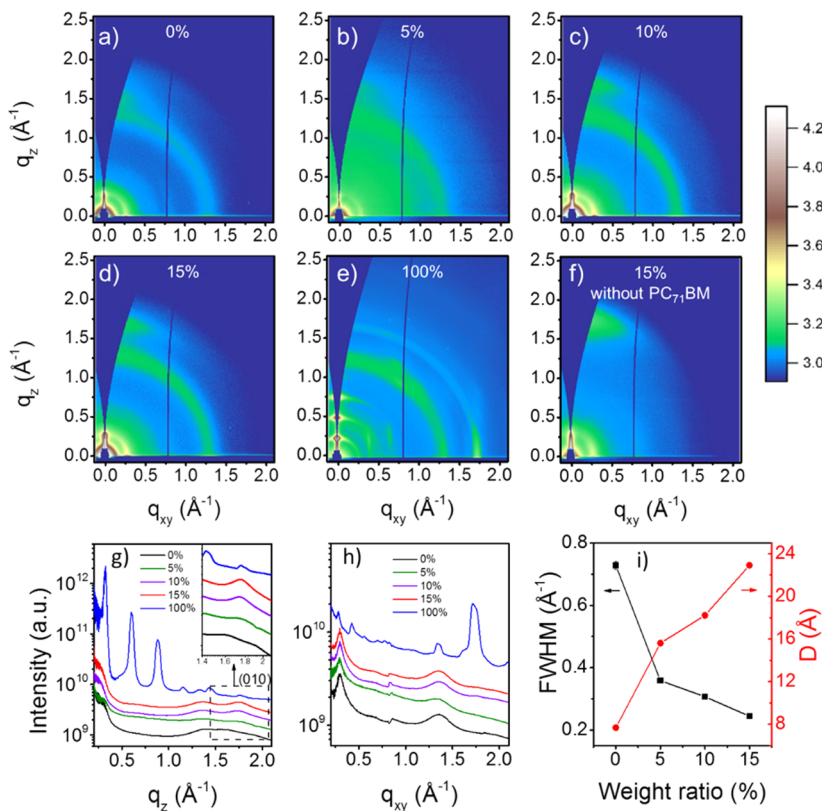


Figure 4. Two-dimensional GIWAXS patterns of the active layer. The weight ratio of p -DTS($FBTTH_2$)₂ is indicated in each image. (a) PTB7-Th:PC₇₁BM (1:1.1), (b) PTB7-Th: p -DTS($FBTTH_2$)₂:PC₇₁BM (0.95:0.05:1.1), (c) PTB7-Th: p -DTS($FBTTH_2$)₂:PC₇₁BM (0.90:0.1:1.1), (d) PTB7-Th: p -DTS($FBTTH_2$)₂:PC₇₁BM (0.85:0.15:1.1), (e) p -DTS($FBTTH_2$)₂:PC₇₁BM (1:1.1), and (f) PTB7-Th: p -DTS($FBTTH_2$)₂ (0.85:0.15). The out-of-plane (g) and in-plane (h) cuts of the corresponding 2D GIWAXS patterns. (010) diffraction peak is enlarged in the inset profile. (i) fwhm of the (010) peak (black symbols) and the correlation length of the $\pi-\pi$ stacking (red symbols).

resonant soft X-ray scattering (R-SoXS) were performed. As shown in Figure 3, the bright and dark regions in the TEM images correspond to the donors and PC₇₁BM-rich domains, respectively.²⁰ These images reveal that all systems show fibrous features with domain sizes of 10–15 nm, thus benefiting exciton separation and charge transport.²¹ However, large domains (approximately 600 nm) are found (Figure 3e) in p -DTS($FBTTH_2$)₂:PC₇₁BM blend film. Blending p -DTS($FBTTH_2$)₂ into PTB7-Th:PC₇₁BM up to 15% does not cause any significant changes in phase separation, which allows for a meaningful discussion on the changes of V_{oc} , J_{sc} , and FF because of the molecular packing. Further R-SoXS studies provide access to the spatial dimensions of phase-separated domains with statistical significance (Figure 3g).^{13,22} The photon energy of 284.2 eV is selected due to the highly enhanced contrast. The PTB7-Th:PC₇₁BM binary blend film shows a scattering peak at $q = 0.2 \text{ nm}^{-1}$, which corresponds to approximately 30 nm characteristics length scale phase separation (domain size is the half of this value, that is, 15 nm), whereas that of the p -DTS($FBTTH_2$)₂:PC₇₁BM blend film exhibits main scattering peaks at $q = 0.01$ and 0.08 nm^{-1} , which corresponds to ~600 nm and ~80 nm characteristics length scale phase separation. The position of the scattering peaks at $q = 0.2 \text{ nm}^{-1}$ do not change obviously after incorporating p -DTS($FBTTH_2$)₂ into the PTB7-Th:PC₇₁BM blend film, indicating that the p -DTS($FBTTH_2$)₂ small molecules have almost no influence on the bicontinuous phase separation in ternary systems. This result is consistent with the TEM results. The phase separation of two donor

materials (PTB7-Th and p -DTS($FBTTH_2$)₂) was studied by means of R-SoXS as well. The scattering profile of the binary donor blend with 15% p -DTS($FBTTH_2$)₂ by weight does not show any peaks in detectable length scale (10–600 nm) nm, thus indicating that these two materials are miscible. It is reasonable to speculate that the small amount p -DTS($FBTTH_2$)₂ will be mixed in PTB7-Th rich phase in the ternary blend. In this overall two phases system, the total scattering intensity TSI (obtained by integrating the scattering profiles over the detectable q range) of the ternary systems was enhanced compared with the PTB7-Th:PC₇₁BM blend film.²³ Thus, the presence of p -DTS($FBTTH_2$)₂ helps with purifying the PTB7-Th rich phase. The pure domains will facilitate the charge transport and reduce bimolecular recombination in the present system.²⁴

Grazing incidence wide-angle X-ray scattering (GIWAXS) is used to probe the molecular stacking and orientation of the active layer.²⁵ Figure 4a-f present the 2D GIWAXS patterns of ternary blends. To quantify the scattering data, the corresponding out-of-plane and in-plane cuts are given in Figure 4g and h, respectively. In the 2D GIWAXS pattern of the pure PTB7-Th thin film (Supporting Information Figure S5), a broad arc-like scattering ($q = 1.73 \text{ \AA}^{-1}$) arises from the Bragg diffraction of periodic PTB7-Th in the out-of-plane direction and corresponds to the $\pi-\pi$ stacking peak. Meanwhile, the $\pi-\pi$ stacking peak ($q = 1.73 \text{ \AA}^{-1}$) is absent in the in-plane direction. This result indicates that the PTB7-Th molecules have a preferred face-on orientation with respect to substrate. By contrast, the 2D GIWAXS pattern of p -DTS($FBTTH_2$)₂ thin film

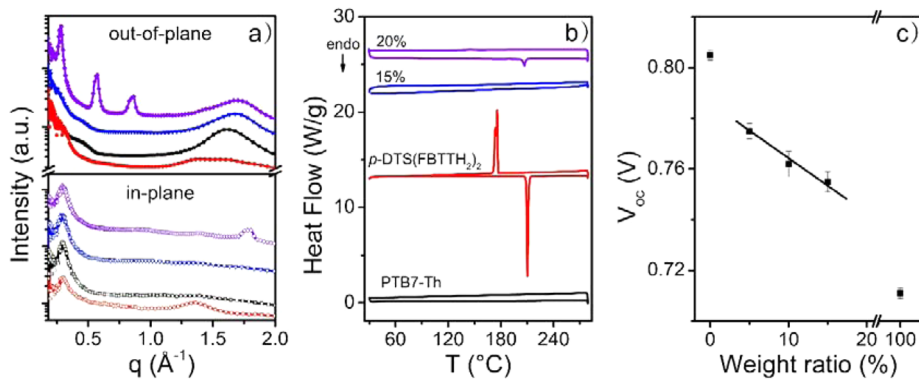


Figure 5. (a) Upper: Out-of-plane scattering of pure PTB7-Th (black), PTB7-Th:PC₇₁BM (100:110, red), PTB7-Th:p-DTS(FBTTH₂)₂ (85:15, blue), PTB7-Th:p-DTS(FBTTH₂)₂ (80:20, violet), and p-DTS(FBTTH₂)₂:PC₇₁BM (15:110, green), respectively. Bottom: In-plane scattering of pure PTB7-Th (black), PTB7-Th:PC₇₁BM (100:110, red), PTB7-Th:p-DTS(FBTTH₂)₂ (85:15, blue) and PTB7-Th:p-DTS(FBTTH₂)₂ (80:20, violet), respectively. (b) DSC curves of PTB7-Th (black), p-DTS(FBTTH₂)₂ (red), PTB7-Th:p-DTS(FBTTH₂)₂ (85:15, blue), PTB7-Th:p-DTS(FBTTH₂)₂ (80:20, violet), respectively. (c) V_{oc} as a function of weight ratio of p-DTS(FBTTH₂)₂.

(Supporting Information Figure S5) exhibits a high degree of molecular ordering in the out-of-plane direction, as evidenced by the strong lamellar (100), (200), and even (300) diffraction peaks. The weak (100) peak and strong (010) peak are present in the in-plane direction. Thus, the p-DTS(FBTTH₂)₂ has a preferential edge-on orientation. Compared with the pure film, the intensity of the face-on π - π stacking peak of the PTB7-Th:PC₇₁BM blend film becomes weaker by addition of PC₇₁BM, (see Figure 5a), which means the PC₇₁BM destroys the crystallinity of PTB7-Th. For the ternary system (Figure 4b, c, and d), the face-on π - π stacking peak (010) becomes more remarkable in the 2D images and sharper in out-of-plane direction through incorporating p-DTS(FBTTH₂)₂ to PTB7-Th, thus indicating an increased ratio of face-on oriented molecules. The strong lamellar (100), (200), and even (300) diffraction peaks are observed at the weight ratio higher than 15% (20% and 30% as shown in Supporting Information Figure S5) due to macrophase separation. However, (100) peak is absent at the weight ratio of p-DTS(FBTTH₂)₂ lower than 15% (Figure 4b–d), which indicates that p-DTS(FBTTH₂)₂ may be mixed into the polymer matrix. We checked the blend of p-DTS(FBTTH₂)₂:PC₇₁BM (15:110) by GIWAXS as well. Supporting Information Figure S6 shows that there are strong (100), (200), and even (300) diffraction peaks of p-DTS(FBTTH₂)₂ in the out-of-plane profile. It means that if the p-DTS(FBTTH₂)₂ is present as an individual phase in the ternary blend at 15%, the diffraction peaks should be detectable by GIWAXS; however, we did not find these peaks (Figure 4g and h). Thus, p-DTS(FBTTH₂)₂ should mix with PTB7-Th. Moreover, from the Differential scanning calorimetry (DSC) results (Figure 5b), it clearly seen that there is no endothermic peak of p-DTS(FBTTH₂)₂ during heating cycle of blend of PTB7-Th and p-DTS(FBTTH₂)₂ with a weight ratio of 15% p-DTS(FBTTH₂)₂ as the pure PTB7-Th. When the macrophase separation takes place (i.e., the weight ratios of 20%), the endothermic peak of the p-DTS(FBTTH₂)₂ appears. These results mean that the p-DTS(FBTTH₂)₂ is not present as an individual phase in the active layer when its weight ratios less than 15%; otherwise, it will crystallize as an individual phase that should be detected by GIWAXS and DSC. On the other hand, compared with pure PTB7-Th, the position of (010) peak is shifted to higher q value, which is located in between that of pure PTB7-Th and that of p-DTS(FBTTH₂)₂ by incorporating 15% p-DTS(FBTTH₂)₂ (Figure 5a), whereas its

position is not changed by adding PC₇₁BM. Because p-DTS(FBTTH₂)₂ does not crystallize below a 15% ratio as indicated by GIWAXS and DSC, the (010) peak of the ternary blends is not originated from the summation of two pure materials. Thus, we propose that an alloy is formed in the present ternary system as represent in Figure 1d. Furthermore, we observed that the V_{oc} does not pin to the donor with high HOMO and the smaller V_{oc} of the corresponding binary blends (Figure 5c), which is consistent with the alloy model.¹⁶ Although small molecules existing as a disordered phase is another possible mechanism,⁹ the shift of (010) peak position and the increase of the crystallinity can only be explained by the alloy model.

Because the incident angle (0.14°) of our measurements is in between the critical angle of the thin film and the substrate, the average information on the whole film is obtained.²⁶ However, we do not find the scattering signals of p-DTS(FBTTH₂)₂ from the 2D GIWAXS patterns (see Figure 4b, c, and d), indicating that the small molecules do not aggregate either on top surface or the bottom of the cells. We changed the incident angle as well. The results are given in Supporting Information Figure S7. It found that the positions of the (010) peak do not change with the incident angle and diffraction from (100), (200), and (300) peaks of the crystallite of small molecules are absent. This means there is no aggregation of small molecules on the top surface, which is consistent with the result get at 0.14° .

The full-width at half-maximum (FWHMs) of the scattering peak, Δq , has a correlation with the nanocrystallite size through the Scherrer equation.²⁷ The FWHMs of the ternary systems were extracted by fitting the out-of-plane cuts with Gaussian equation (Supporting Information Figure S8). The (010) coherence lengths of the reference cell and ternary system were calculated by using Scherrer analysis. The correlation length is increased from ~ 8 Å to ~ 23 Å (Figure 4i) when p-DTS(FBTTH₂)₂ increases from 0% to 15%, which indicates that large nanocrystallite sizes are formed along the π - π stacking direction in the ternary system (Figure 1d). As a result, charge carrier mobilities and charge collection efficiencies might be enhanced.

In the present case, the domain size of the ternary system and the reference PTB7-Th:PC₇₁BM are similar to each other in terms of TEM and R-SoXS results, which makes the discussion on working mechanism meaningful. Compared with the reference PTB7-Th:PC₇₁BM binary device, the ternary

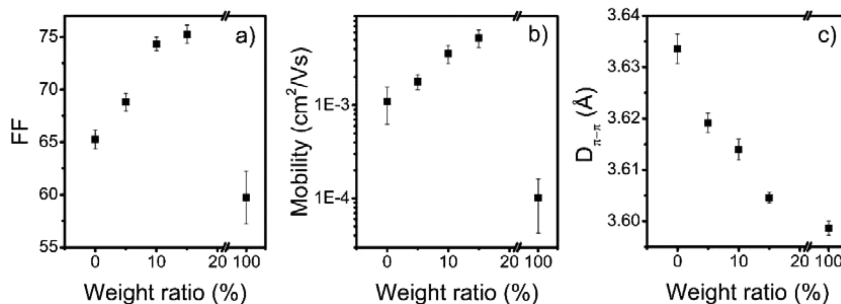


Figure 6. (a) FF, (b) hole mobility, and (c) distance of the $\pi-\pi$ stacking at different weight ratios of $p\text{-DTS}(\text{FBTTH}_2)_2$.

system achieves a higher FF. The variation of FF as the function of composition is presented in Figure 6a. The importance of mobility for good FF has been recently illustrated.²⁸ To elucidate the reason, the hole mobility of the ternary system was measured using the space-charge limited current (SCLC) regime of a hole-only diode device configuration (Supporting Information Figure S9). Figure 6b shows the hole mobility as a function of the weight ratio of $p\text{-DTS}(\text{FBTTH}_2)_2$. The hole mobility of the PTB7-Th is larger than $p\text{-DTS}(\text{FBTTH}_2)_2$. The hole mobilities of the ternary system are increased through the incorporation of $p\text{-DTS}(\text{FBTTH}_2)_2$, which is attributed to a high degree of ordering and face-on $\pi-\pi$ stacking as demonstrated in GIWAXS. In addition, the $\pi-\pi$ stacking distance shows an inverse relationship with hole mobility.²⁸ The variation of $\pi-\pi$ stacking distance with the weight ratio of $p\text{-DTS}(\text{FBTTH}_2)_2$ is presented in Figure 6c. Compared with the PTB7-Th:PC₇₁BM binary device, the $\pi-\pi$ stacking distance of the ternary system shortens as the weight ratio of $p\text{-DTS}(\text{FBTTH}_2)_2$ increases, thus possibly leading to a high FF as demonstrated in previous works.²⁹ Thus, we attribute the high FF of the ternary system to high mobility, face-on $\pi-\pi$ stacking, short $\pi-\pi$ stacking distance, and relatively pure domains indicated by R-SoXS. However, $p\text{-DTS}(\text{FBTTH}_2)_2$ may have the shortest $\pi-\pi$ stacking distance, but $p\text{-DTS}(\text{FBTTH}_2)_2$ does not show highest FF because of low hole mobility.

CONCLUSION

To summarize, high performance ternary solar cells with an average PCE of 10.5% have been designed and fabricated, thus showing a suitably designed ternary blend that has the potential for higher cell efficiency than binary blends. In the present system, two miscible donor molecules form an alloy, that is, a small molecule with high crystallinity was incorporated with a polymer that had a preferential face-on $\pi-\pi$ stacking. The crystallinity and the face-on orientation of the ternary system are enhanced through the incorporation of a high-crystalline small molecule, resulting in high hole mobility and less charge recombination. Thus, the J_{sc} , FF, and PCE are enhanced. Our approach provides a facile ternary strategy to increase the FF and J_{sc} simultaneously and is proved to be an efficient strategy for fabricating OSCs with high performance.

EXPERIMENTAL SECTION

Device Fabrication and Characterization. PTB7-Th and $p\text{-DTS}(\text{FBTTH}_2)_2$ were purchased from 1-Material Chemscitech Inc. (Canada) and used as received. The ZnO precursor solution was prepared by dissolving 0.14 g of zinc acetate dihydrate ($\text{Zn}(\text{CH}_3\text{COO})_2 \cdot 2\text{H}_2\text{O}$, 99.9%, Aldrich, U.S.A.) and

0.5 g of ethanolamine ($\text{NH}_2\text{CH}_2\text{CH}_2\text{OH}$, 99.5%, Aldrich, U.S.A.) in 5 mL of 2-methoxyethanol ($\text{CH}_3\text{OCH}_2\text{CH}_2\text{OH}$, 99.8%, J&K Scientific, Canada). Patterned ITO glass with a sheet resistance of $15 \Omega \text{ sq}^{-1}$ was purchased from CSG HOLDING Co., Ltd. (China). The ITO glass was cleaned by sequential sonifications in soap DI water, DI water, acetone, and isopropanol for 15 min at each step. After ultraviolet/ozone (Ultraviolet Ozone Cleaner, Jelight Company, U.S.A.) treatment for 4 min, a ZnO electron transport layer was prepared through spin coating at 3000 rpm from a ZnO precursor solution. Then the ZnO substrates were immediately baked in air at 200 °C for 30 min. Active layer solutions (D/A ratio 1:1.1) with polymer concentrations of 10 mg mL^{-1} were prepared in chlorobenzene (CB) with 3% (volume fraction) of DIO. Active layers were spin coated from the polymer solution on the substrate in a N_2 glovebox at 1500 rpm to obtain thicknesses of approximately 100 nm. At a vacuum level of approximately $1.0 \times 10^{-6} \text{ mbar}$, a thin layer (5 nm) of MoO_x was deposited as the anode interlayer, and 100 nm of Ag was deposited as the top electrode. Device $J-V$ characteristics were measured under AM1.5G (100 mW/cm²) using a Newport Thermal Oriel 91159A solar simulator. Light intensity is calibrated with a Newport Oriel PN 91150 V Si-based solar cell. $J-V$ characteristics were recorded using a Keithley 2400 source meter unit. Typical cells have device areas of approximately 4 mm². A mask with well-defined area was used to measure the $J-V$ characteristics as well. All the masked and unmasked tests had consistent results with relative errors within 5%. EQEs were performed in air with an Oriel Newport system (Model 66902) equipped with a standard Si diode. Monochromatic light was generated from a Newport 300W lamp source.

Other Characterizations. UV-vis absorption spectra were acquired on a Lambda 950 spectrophotometer (PerkinElmer, U.S.A.). The hole mobility was measured via the SCLC method by using a device architecture of ITO/PEDOT:PSS/active layer/ MoO_x /Ag by acquiring the current–voltage curves and fitting the results to a space-charge limited form. The thicknesses of the active layer were measured by using an Alpha-atepD-120 stylus profilometer, Kla-Tencor. The DSC data were obtained from DSC Q100 TA Instruments, U.S.A. The heating rate was 10 K/min. GIWAXS measurements were performed at beamline 7.3.3 at the Advanced Light Source,³⁰ Berkeley, U.S.A. GIWAXS samples were prepared on Si substrates coated with ZnO layer using identical blend solutions as those used in devices. The incident angle was 0.14°, which maximized the scattering intensity from the samples. The scattered X-rays were detected by using a Dectris Pilatus 2 M photon counting detector. R-SoXS transmission measurements were performed at beamline 11.0.1.2 at the ALS.³¹ Samples for R-SoXS measurements were prepared on a PEDOT:PSS

modified glass/ITO substrate under the same conditions as those used for device fabrication and then transferred by floating in water to a 1.5 mm × 1.5 mm, 100 nm thick Si₃N₄ membrane (Norcada Inc.). Two-dimensional scattering patterns were collected on an in-vacuum CCD camera (Princeton Instrument PI-MTE). The beam size at the sample is 100 nm by 200 nm.

ASSOCIATED CONTENT

Supporting Information

Additional cyclic voltammograms, optical microscopy images, certificate of power conversion efficiency, UV-vis absorption spectra, GIWAXS, and an example of Gaussian fitting and SCLC data. The Supporting Information is available free of charge on the ACS Publications website at DOI: 10.1021/jacs.5b03449.

AUTHOR INFORMATION

Corresponding Authors

*msewma@mail.xjtu.edu.cn
*weizx@nanoctr.cn

Notes

The authors declare no competing financial interest.

ACKNOWLEDGMENTS

We acknowledge the financial support by the National Natural Science Foundation of China (Grant Nos. 21125420 and 91427302) and the “Strategic Priority Research Program” of the Chinese Academy of Sciences (Grant No. XDA0909040200). X-ray data was acquired at beamlines 7.3.3 at the Advanced Light Source, which is supported by the Director, Office of Science, Office of Basic Energy Sciences, of the U.S. Department of Energy under Contract No. DE-AC02-05CH11231.

REFERENCES

- (a) Dou, L.; You, J.; Hong, Z.; Xu, Z.; Li, G.; Street, R. A.; Yang, Y. *Adv. Mater.* **2013**, *25*, 6642–6671. (b) Service, R. F. *Science* **2011**, *332*, 293–293.
- (a) Cheng, Y. J.; Yang, S. H.; Hsu, C. S. *Chem. Rev.* **2009**, *109*, 5868–5923. (b) Li, Y. F. *Acc. Chem. Res.* **2012**, *45*, 723–733. (c) Boudreault, P.-L. T.; Najari, A.; Leclerc, M. *Chem. Mater.* **2010**, *23*, 456–469.
- (a) Li, G.; Shrotriya, V.; Huang, J. S.; Yao, Y.; Moriarty, T.; Emery, K.; Yang, Y. *Nat. Mater.* **2005**, *4*, 864–868. (b) Peet, J.; Kim, J. Y.; Coates, N. E.; Ma, W. L.; Moses, D.; Heeger, A. J.; Bazan, G. C. *Nat. Mater.* **2007**, *6*, 497–500.
- (a) Li, G.; Chu, C. W.; Shrotriya, V.; Huang, J.; Yang, Y. *Appl. Phys. Lett.* **2006**, *88*, 253503. (b) Kim, J. Y.; Lee, K.; Coates, N. E.; Moses, D.; Nguyen, T.-Q.; Dante, M.; Heeger, A. J. *Science* **2007**, *317*, 222–225. (c) He, Z.; Zhong, C.; Huang, X.; Wong, W.-Y.; Wu, H.; Chen, L.; Su, S.; Cao, Y. *Adv. Mater.* **2011**, *23*, 4636–4643.
- (a) Liao, S.-H.; Jhuo, H.-J.; Yeh, P.-N.; Cheng, Y.-S.; Li, Y.-L.; Lee, Y.-H.; Sharma, S.; Chen, S.-A. *Sci. Rep.* **2014**, *4*, 6813. (b) Liu, Y.; Zhao, J.; Li, Z.; Mu, C.; Ma, W.; Hu, H.; Jiang, K.; Lin, H.; Ade, H.; Yan, H. *Nat. Commun.* **2014**, *5*, 5293.
- Chen, C.-C.; Chang, W.-H.; Yoshimura, K.; Ohya, K.; You, J.; Gao, J.; Hong, Z.; Yang, Y. *Adv. Mater.* **2014**, *26*, 5670–5677.
- Ameri, T.; Khoram, P.; Min, J.; Brabec, C. J. *Adv. Mater.* **2013**, *25*, 4245–4266.
- (a) Lu, L.; Xu, T.; Chen, W.; Landry, E. S.; Yu, L. *Nat. Photonics* **2014**, *8*, 716–722. (b) Zhang, Y.; Deng, D.; Lu, K.; Zhang, J.; Xia, B.; Zhao, Y.; Fang, J.; Wei, Z. *Adv. Mater.* **2015**, *27*, 1071–1076.
- (a) Koppe, M.; Egelhaaf, H.-J.; Clodic, E.; Morana, M.; Lüer, L.; Troeger, A.; Sgobba, V.; Guldi, D. M.; Ameri, T.; Brabec, C. J. *Adv. Energy Mater.* **2013**, *3*, 949–958. (b) Koppe, M.; Egelhaaf, H.-J.; Dennler, G.; Scharber, M. C.; Brabec, C. J.; Schilinsky, P.; Hoth, C. N. *Adv. Funct. Mater.* **2010**, *20*, 338–346.
- Jørgensen, M.; Norrman, K.; Krebs, F. C. *Sol. Energy Mater. Sol. Cells* **2008**, *92*, 686–714.
- (a) Hoppe, H.; Sariciftci, N. S. *J. Mater. Chem.* **2006**, *16*, 45–61. (b) Chen, L.-M.; Hong, Z.; Li, G.; Yang, Y. *Adv. Mater.* **2009**, *21*, 1434–1449. (c) Graham, K. R.; Cabanatos, C.; Jahnke, J. P.; Idso, M. N.; El Labban, A.; Ndjawa, G. O. N.; Heumueller, T.; Vandewal, K.; Salleo, A.; Chmelka, B. F.; Amassian, A.; Beaujuge, P. M.; McGehee, M. D. *J. Am. Chem. Soc.* **2014**, *136*, 9608–9618.
- Sepe, A.; Rong, Z. X.; Sommer, M.; Vaynzof, Y.; Sheng, X. Y.; Muller-Buschbaum, P.; Smilgies, D. M.; Tan, Z. K.; Yang, L.; Friend, R. H.; Steiner, U.; Huttner, S. *Energy Environ. Sci.* **2014**, *7*, 1725–1736.
- Rivnay, J.; Mannsfeld, S. C. B.; Miller, C. E.; Salleo, A.; Toney, M. F. *Chem. Rev.* **2012**, *112*, 5488–5519.
- (a) Kline, R. J.; McGehee, M. D.; Toney, M. F. *Nat. Mater.* **2006**, *5*, 222–228. (b) Salleo, A.; Kline, R. J.; DeLongchamp, D. M.; Chabinyc, M. L. *Adv. Mater.* **2010**, *22*, 3812–3838. (c) Chabinyc, M. L. *Polym. Rev.* **2008**, *48*, 463–492.
- Nguyen, T. L.; Choi, H.; Ko, S.-J.; Uddin, M. A.; Walker, B.; Yum, S.; Jeong, J.-E.; Yun, M. H.; Shin, T.; Hwang, S.; Kim, J. Y.; Woo, H. Y. *Energy Environ. Sci.* **2014**, *7*, 3040–3051.
- (a) Khlyabich, P. P.; Burkhardt, B.; Thompson, B. C. *J. Am. Chem. Soc.* **2012**, *134*, 9074–9077. (b) Khlyabich, P. P.; Rudenko, A. E.; Street, R. A.; Thompson, B. C. *ACS Appl. Mater. Interfaces* **2014**, *6*, 9913–9919. (c) Street, R. A.; Davies, D.; Khlyabich, P. P.; Burkhardt, B.; Thompson, B. C. *J. Am. Chem. Soc.* **2013**, *135*, 986–989.
- (a) Liao, S.-H.; Jhuo, H.-J.; Cheng, Y.-S.; Chen, S.-A. *Adv. Mater.* **2013**, *25*, 4766–4771. (b) He, Z.; Xiao, B.; Liu, F.; Wu, H.; Yang, Y.; Xiao, S.; Wang, C.; Russell, T. P.; Cao, Y. *Nat. Photonics* **2015**, *9*, 174–179.
- (a) Love, J. A.; Proctor, C. M.; Liu, J.; Takacs, C. J.; Shareko, A.; van der Poll, T. S.; Heeger, A. J.; Bazan, G. C.; Nguyen, T.-Q. *Adv. Funct. Mater.* **2013**, *23*, 5019–5026. (b) Perez, L. A.; Chou, K. W.; Love, J. A.; van der Poll, T. S.; Smilgies, D.-M.; Nguyen, T.-Q.; Kramer, E. J.; Amassian, A.; Bazan, G. C. *Adv. Mater.* **2013**, *25*, 6380–6384.
- Sun, Y.; Seo, J. H.; Takacs, C. J.; Seifter, J.; Heeger, A. J. *Adv. Mater.* **2011**, *23*, 1679–1683.
- (a) Ma, W.; Kim, J. Y.; Lee, K.; Heeger, A. J. *Macromol. Rapid Commun.* **2007**, *28*, 1776–1780. (b) Su, M.-S.; Kuo, C.-Y.; Yuan, M.-C.; Jeng, U. S.; Su, C.-J.; Wei, K.-H. *Adv. Mater.* **2011**, *23*, 3315–3319.
- (a) Chen, H.-Y.; Hou, J.; Zhang, S.; Liang, Y.; Yang, G.; Yang, Y.; Yu, L.; Wu, Y.; Li, G. *Nat. Photonics* **2009**, *3*, 649–653. (b) Liang, Y.; Xu, Z.; Xia, J.; Tsai, S.-T.; Wu, Y.; Li, G.; Ray, C.; Yu, L. *Adv. Mater.* **2010**, *22*, E135–E138.
- (a) Ma, W.; Tumbleston, J. R.; Wang, M.; Gann, E.; Huang, F.; Ade, H. *Adv. Energy Mater.* **2013**, *3*, 864–872. (b) Chen, W.; Nikiforov, M. P.; Darling, S. B. *Energy Environ. Sci.* **2012**, *5*, 8045–8074.
- Ma, W.; Tumbleston, J. R.; Ye, L.; Wang, C.; Hou, J.; Ade, H. *Adv. Mater.* **2014**, *26*, 4234–4241.
- Stuart, A. C.; Tumbleston, J. R.; Zhou, H.; Li, W.; Liu, S.; Ade, H.; You, W. *J. Am. Chem. Soc.* **2013**, *135*, 1806–1815.
- Müller-Buschbaum, P. *Adv. Mater.* **2014**, *26*, 7692–7709.
- (a) Tolan, M. *X-Ray Scattering from Soft-Matter Thin Films. Materials Science and Basic Research*; Springer: Berlin/Heidelberg, 1999; pp 7. (b) Zhang, J. Q.; Posselt, D.; Smilgies, D. M.; Perlitz, J.; Kyriakos, K.; Jakobs, S.; Papadakis, C. M. *Macromol. Rapid Commun.* **2014**, *35*, 1622–1629.
- Smilgies, D.-M. *J. Appl. Crystallogr.* **2009**, *42*, 1030–1034.
- Albrecht, S.; Tumbleston, J. R.; Janietz, S.; Dumsch, I.; Allard, S.; Scherf, U.; Ade, H.; Neher, D. *J. Phys. Chem. Lett.* **2014**, *5*, 1131–1138.
- Szarko, J. M.; Guo, J.; Liang, Y.; Lee, B.; Rolczynski, B. S.; Strzalka, J.; Xu, T.; Loser, S.; Marks, T. J.; Yu, L.; Chen, L. X. *Adv. Mater.* **2010**, *22*, 5468–5472.

(30) (a) Krebs, F. C.; Jørgensen, M.; Norrman, K.; Hagemann, O.; Alstrup, J.; Nielsen, T. D.; Fyenbo, J.; Larsen, K.; Kristensen, J. *Sol. Energy Mater. Sol. Cells* **2009**, *93*, 422–441. (b) Hexemer, A.; Bras, W.; Glossinger, J.; Schaible, E.; Gann, E.; Kirian, R.; MacDowell, A.; Church, M.; Rude, B.; Padmore, H. *J. Phys. Conf. Ser.* **2010**, *247*, 012007.

(31) Gann, E.; Young, A. T.; Collins, B. A.; Yan, H.; Nasiatka, J.; Padmore, H. A.; Ade, H.; Hexemer, A.; Wang, C. *Rev. Sci. Instrum.* **2012**, *83*, 045110.